

Application of *Aloe vera* Gel Blended Polymer-Collagen Scaffolds for Bone Tissue Engineering

Marwa Abdul Muhsien Hassan^{1✉}, Asmaa Hadi Mohammed², Ekhlas Majeed Hameed³

¹Department of Physics, College of Science, Mustansiriyah University, Baghdad, Iraq

²Department of Physics, College of Science, Al-Nahrain University, Baghdad, Iraq

³College of Medical, University of Wasit, Wasit, Iraq

✉ Corresponding author. E-mail: marwamedicalphysics@uomustansiriyah.edu.iq; marwamedicalphysics@gmail.com

Received: May 22, 2022; **Revised:** Feb. 18, 2023; **Accepted:** Apr. 3, 2023

Citation: M.A.M. Hassan, A.H. Mohammed, E.M. Hameed. Application of *Aloe vera* gel blended polymer-collagen scaffolds for bone tissue engineering. *Nano Biomedicine and Engineering*, 2023.

<http://doi.org/10.26599/NBE.2023.9290016>

Abstract

Osteoblasts have an essential role in the process of bone formation, and polymer-collagen-*Aloe vera* (AV) is known to stimulate osteoblast proliferation and maturation. In this translational study, the effects of scaffolds on bone healing and the potential mechanisms responsible were investigated using an animal model of bone defects. Here, following surgical introduction of a bone defect in the proximal femurs of male rabbits, the left femur was implanted with scaffolds for 21 days, then compared to the right femur, which served as a control. According to histological analyses, the use of scaffolds did not result in hepatotoxicity or nephrotoxicity. In contrast to the control group, imaging using X-ray transmission and microcomputed tomography revealed that scaffold implantation boosted the bone repair. In addition, microcomputed tomographic and bone histomorphometric assays in the scaffold-treated group exposed an expansion in the formation of new trabecular bone. Furthermore, scaffold implantation resulted in a considerable increase in trabecular bone thickness but a decrease in the trabecular parameter factor. Following scaffold implantation, the quantities of alkaline phosphatase and osteocalcin, biomarkers capable of simulating bone development, were found to have gradually increased. Overall, this translational study found that scaffolds can improve bone repair by increasing trabecular bone creation via upregulation of Runx2-mediated alkaline phosphatase and osteocalcin gene expression. Our findings therefore suggest that scaffolds can be used to treat bone problems such as deformities and fractures.

Keywords: *Aloe vera*; polymer-collagen scaffolds; bone tissue engineering

Introduction

Biomaterial-based techniques can be employed to promote the regeneration of injured tissues and have therefore become promising alternatives to existing surgical and medicinal therapies [1–3]. The development of scaffolds and biomaterials capable of encouraging and guiding the growth of new healthy tissue is important for the field of bone regeneration,

due to the increasing incidence of bone loss and damage brought on by traumatic or pathological conditions [1, 2].

Artificial scaffolds, a class of synthetic materials including ceramics, polymers, metals, and composites, have been tested to determine whether they can facilitate osteogenesis [3–8]. The material composition of scaffolds is a critical determinant of bone growth. However, porous scaffolds with

targeted osteogenesis have become significantly better in recent years [9–11]. To enhance osteogenesis and angiogenesis, macroporosity (i.e., pore sizes greater than 100 μm in diameter) is frequently necessary [12]. To increase circulation of fluids and cell migration to the core of the implant, interconnected macropores are required [13]. In addition, microporosity (i.e., pore sizes under 10 μm in diameter) also plays a vital role in scaffold osteoinduction. Scaffold chemical composition is also a crucial determinant of osteogenic activity [6, 10]. Some scaffolds, despite having similar chemical compositions, are osteoinductive, while others are not [11–14]. Micro porous hydroxyapatite (HAP) ceramics, in particular, have been found to stimulate bone growth in dogs following intramuscular implantation, but formulations with insufficient microporosity did not enhance bone growth [13]. As a result, specific microporosity requirements are essential for effective scaffold osteoinduction [14].

On the other hand, excessive microporosity has also been shown to be detrimental to the mechanical characteristics of scaffolds [15]. In addition to adequate microporosity, a perfect scaffold should also have satisfactory mechanical qualities (i.e., stiffness, strength, and toughness), since the scaffold can only preserve its shape and offer support after insertion and during bone formation if it has the correct mechanical properties [16–18].

Bone grafts and implantations are widespread in veterinary medicine, where they are commonly used for treating various fracture complications (e.g., delayed union and nonunion), or may be used in the treatment of pathological fractures. Moreover, they are also used to provide stability, promote healing, and fill osseous defects of cavities. Several methods have been used for fracture repair, including the use of internal bone plates, bone pins, surgical wires, bone screws, and external devices. In addition, some authors have used chemical agents such as PGF2a to promote fracture healing in dogs, or have used PGE2 to enhance bone reabsorption of bony tubular splints during the bone remodeling phase in rabbits [19]. At present, treatments used to facilitate fracture healing include lasers, stem cells, growth factors, extracorporeal shock waves, and supplementation with platelet-rich plasma. The goal of fracture healing is to regenerate mineralized tissue at the fracture site, to restore the mechanical strength and integrity of the injured bone, and to normalize the functionality of the

repaired tissue. Some fractures feature bone loss; this is found in many pathological fractures resulting from bone disease (e.g., osteosarcoma), in fracture complications such as delayed union or nonunion, and in fractures due to gunshot wounds that lead to bone loss. Such fractures may require treatment using different forms of grafting and/or implantation treatment [19–22].

In this study, we examine the role of *Aloe vera* (AV) in polymer-collagen scaffolds for osteogenesis and bone regeneration.

Methods

Preparation of poly-L/D-lactic acid (PLDLA)-collagen scaffolds

Scaffold pore size was adjusted granulometrically to 250–500 μm using PLDLA-collagen dissolution in chloroform (0.1, 0.7 g/mL). The resulting solution was then poured into a 5 mm diameter silicon cylindrical mold and held until the solvent had completely evaporated. To remove sucrose particles, cylindrical samples (5 mm \times 5 mm) were punched out of the molds and placed in a 1% polyvinyl alcohol (PVA) solution. PLDLA, poly-L/lactic acid (PLLA), and PLLA-collagen scaffolds were then cut to a diameter of 5 mm and a thickness of 3 mm. These PLDLA-collagen scaffolds were then disinfected in 70% ethanol for 30 min before being subjected to ultraviolet (UV) radiation for another 30 min on each side. To separate the water-soluble fraction (which is rich in acetylated polysaccharides) from the cellulose-rich solid fraction, commercial *Aloe vera* juice was centrifuged at 3 000 r/min for 15 min. The water-soluble fraction (supernatant) was used to coat structures, since it contains bioactive polysaccharides, phenolic compounds, soluble carbohydrates, proteins, and minerals, as well as bioactive polysaccharides. The pH of the supernatant was approximately 4. The presence of several organic acids (e.g., acetic acid, lactic acid, and succinic acid) explains the extracts' somewhat acidic nature. Via pH modification, three types of *Aloe vera* extract samples were obtained: a pH = 3 solution (adjusted using with 0.018 mol/L HCl), a pH = 5 solution (adjusted using 0.5 mol/L NaOH), and a pH = 4 gel, which was used directly as obtained. Next, each scaffold was immersed in 1 mL of *Aloe vera* extract solution and agitated for 3 h to allow interaction between the functional groups

generated on surface of the scaffold and the functional groups in the polysaccharide structures. After 3 h, the samples were washed with 70% ethanol to eliminate residual *Aloe vera* that had failed to adhere to the surface. In addition, since polysaccharides are insoluble in ethanol, their precipitation aids in adhesion to the coating of the scaffold surface.

Animals

Rabbits were obtained from the National Center for Drug Control and Research (NCDCR) of the Ministry of Health. Before the operation, rabbits were kept in three special cages for seven days. All animals were given an antiparasitic medicine (Ivermectin, 0.1 mg/kg) to prevent internal and external parasites. During the operation, an induced surgical transverse fracture was produced to remove roughly 1 cm of femur length near the mid-shift of the femoral bone. The femoral gap was then filled with a sufficiently-sized scaffold implant fastened with an intramedullary pin as an internal fixation device. The animals were divided into groups based on the scaffold treatment they received ($n = 40$ for each group). Before surgery, all instruments, towels, and appliances were autoclaved at (49.5 °C) and 2 MPa for 30 min. Research ethics approval (license No. 13/2020) was obtained for the animal research facilities as issued to the Department of Physics, College of Science, Mustansiriyah University by the Ministry of Health, NCDCR, Iraq.

Anesthesia and creation of bone fractures

Prior to the operation, rabbits were kept for 12 h without food and 2 h without drink. Intramuscular injections of 2% xylazine hydrochloride (17.5 mg/kg), 5% ketamine hydrochloride (25 mg/kg), and 0.5 mL of lidocaine along the incision site provided general anesthesia. The antibiotic and anesthetic doses were determined using

$$\text{Dose} = \frac{\text{Animals mass} \times \text{dose rate}}{\text{Constriction of drug}} \quad (1)$$

The surgical field (i.e., the thigh region from the hip joint to the stifle joint) was prepared for aseptic surgical operation by cutting and shaving fur, washing the area with soap and tap water, and disinfection with 70% prepared alcohol. Surgical tools, sutures, electric saw, curtains, goggles, and surgical gloves were all introduced as necessary for

the surgery. The experiment was conducted on 40 healthy adult rabbits weighing 2–2.5 kg and ranging in age from 12 to 18 months.

Surgical protocol

Following anesthetic induction, animals were positioned in lateral recumbence and the body was draped in sterile drapes, with the exception of the surgical field, which was coated with cotton embedded with alcohol and dabbed with a 2% iodine tincture. The lateral aspect of the thigh region was surgically incised about 4 cm from the great trochanter to the lateral side of the patella. Bleeding was routinely stopped, the subcutaneous tissue was dissected, the fascia lata was sharply dissected, and the underlying biceps femoralis and vastus lateralis muscles were bluntly separated to expose the femoral mid-shift. Next, using curved and fine artery forceps, the tissue around the femoral bone was dissected at the fracture site to separate abducted muscle. Next, soft tissues adjacent to the bone were protected with two curved scissors, and an electrical saw was used to remove about 1 cm of the femoral shaft while cooling the bone with sterile normal saline. Next, a scaffold of the appropriate size was implanted in the empty space in the femur. Intramedullary pins of 2.25–2.5 mm in diameter were used as internal fixing methods to attach the scaffold to the two femoral bone pieces during implantation. The pins were inserted using a retrograde pin choke method. Penicillin powder was then applied as a local antibiotic and the muscles and fascia lata were then sutured in a simple continuous pattern using 2/0 chromic cat gut. The skin was then closed in a simple interrupted pattern using 2/0 non-absorbing silk. The excess portion of the pin was reduced using a pin cutter as soon as possible after the procedure to ensure the position and location of the intramedullary pins and their proper implantation in the bone.

Cell culture

L3T3 mouse fibroblasts were grown in Dulbecco's modified Eagle's medium (DMEM) with 10% fetal bovine serum, 100 units/mL penicillin, and 100 units/mL streptomycin at 37 °C in a 5% CO₂ humidified environment. The culture medium was replaced every three days. Next, scaffolds with a total surface area of 1 cm² and a thickness of 2 mm were placed in 12-well culture plates for *in vitro* biocompatibility testing. The scaffold samples were sterilized under UV light for 2 h, and then soaked in a

75% alcohol solution overnight before seeding with cells. The specimens were washed three times with phosphate buffered saline (PBS) for 30 min each time, and then washed twice with cell culture media. The cell compatibility and cytotoxicity of L3T3 murine fibroblasts (3104) planted onto scaffolds in the culture medium were then evaluated.

Cell viability

The number of live cells was determined using an 3-dimethylthiazol-2,5-diphenyltetrazolium bromide (MTT) colorimetric test after 24, 48, and 72 h of cell seeding in the presence or absence of scaffolds. To allow for formazan crystal formation, cultures in tissue culture polystyrene plate (TCP) and test scaffolds were rinsed twice in PBS then incubated with MTT (0.5 mg/mL in DMEM without phenol red) at 37 °C for 4 h. The supernatant was then collected, and 200 μ L of dimethyl sulfoxide (DMSO) was added for 30 min at 37 °C to dissolve formazan crystals. After full dissolution, the optical density of the supernatant solution was measured at 540 nm using a microplate reader. Wells that did not have scaffolds served as negative controls. All data were expressed statistically using the mean and standard deviation ($n = 3$).

Immunohistological analyses of alkaline phosphatase (ALP) and osteocalcin (OCN)

Immunohistology was used to examine the effects of scaffolds on ALP and OCN levels at bone defect locations. The animals were slaughtered 21 days after scaffold implantation. The femurs were then removed and collected. Femur specimen slices were created by first fixing samples for 10 min at 20 °C with a fixing reagent (i.e., ratio of acetone and methanol is 1 : 1) then incubating them for 15 min at room temperature with 0.2% Triton X-100. Polyclonal antibodies against rabbit ALP and OCN were used to detect ALP and OCN in bone samples after incubation at 4 °C overnight. After washing, slices were left at room temperature for 1 h to react with the secondary antibody. After reacting with 3,3'-diaminobenzidine, stained portions were visible. Using a light microscope, the specimen slices were examined and photographed.

Immunoblotting analyses of ALP and OCN

After treatment, proteins were prepared from control and scaffold-treated femurs in an ice-cold radioimmunoprecipitation assay buffer (i.e., 25 mmol/L

tris-HCl (pH = 7.2), 0.1% sodium dodecylsulfate (SDS), 1% Triton X-100, 1% sodium deoxycholate, 0.15 mol/L NaCl, and 1 mmol/L ethylene diamine tetraacetic acid (EDTA)). To avoid protein degradation, a mixture of proteinase inhibitors, including 1 mmol/L phenyl methyl sulfonyl fluoride, 1 mmol/L sodium orthovanadate, and 5 mg/mL leupeptin, was added to the radioimmunoprecipitation assay buffer. Protein concentrations were then quantified by a bicinchoninic acid protein assay kit. Cytosolic proteins (100 μ g/well) were subjected to SDS-polyacrylamide gel electrophoresis (PAGE), then transferred to nitrocellulose membranes. These membranes were blocked with 5% non-fat milk at 37 °C for 1 h. ALP and OCN were then immunodetected using antibodies. As an internal control, a mouse monoclonal antibody (Sigma-Aldrich) was used to detect actin. Digital imaging equipment was used to quantify these protein bands.

Statistical analysis

All statistical analyses were performed using GraphPad version 5.0. Findings were reported as mean standard error of the mean and subjected to analyses of variance followed by Newman-Keuls post-hoc tests. P values < 0.05 were judged to be statistically significant. All histology findings were presented in a qualitative manner.

Results

The MTT assay was used to assess the biocompatibility of the composite scaffolds. It measures cellular metabolic activity, which is directly proportional to the number of live cells. The cell viability results relative to a control group are shown in Fig. 1. These data showed an increase in cell number from day 1 to day 3. On day 1, the number of cells in the medium containing the polymer-COL-AV composite scaffold was nearly equal to those of cells exposed to the polymer-COL, AV, and the control. We did not observe statistically significant differences between these values on day 1 ($P > 0.05$), and this finding demonstrates that adding *Aloe vera* to the polymer-COL scaffold did not affect survivability. On day 3, the polymer-COL-AV group showed a significant increase in cell number, which may be due to glycoproteins in the *Aloe vera* gel, since this has been shown to stimulate cell proliferation and promote growth in human

fibroblasts. Moreover, anthroquinones (i.e., aloemodin) are known to have antioxidant- and free radical-scavenging properties. Furthermore, the addition of the AV gel also increased the hydrophilic quality of the scaffold, allowing it to inflate into the culture medium and promote cell infusion into the three-dimensional (3D) structure, resulting in greater adhesion and proliferation. The increased swelling also allowed the scaffold sample to better absorb nutrients from the culture media. Thus, by adding AV to the polymer-COL scaffold, biological properties were altered, creating a favorable environment for cell adhesion, growth, and proliferation.

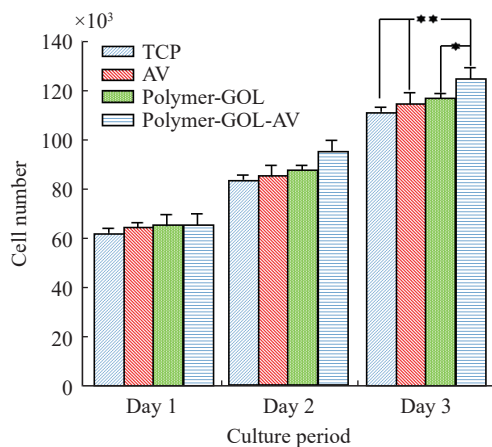


Fig. 1 MTT assay of fibroblast cells cultured on polymer-COL, polymer-COL-AV, and TCP. Error bars represent mean \pm standard deviation (SD) ($n = 3$); * $P < 0.05$ and ** $P < 0.01$.

Administration of polymer-GOL-AV scaffolds did not cause hepato- or nephrotoxicity

Histological investigations were conducted to assess the toxicity of the scaffolds to animal tissue (Fig. 2). After implanting scaffolds into femur bone defect locations for 21 days, histological examinations revealed that scaffold implantation had no effect on hepatocyte morphology or cell configurations in the liver (Fig. 2(a)). Similarly, the implantation of scaffolds did not result in nephrotoxicity (Fig. 2(b)). Tissue sections revealed normal appearance of the renal cortex, which is made up of glomeruli and renal tubules (i.e., proximal, distal convoluted tubules, and collecting tubules) (Fig. 2(b)). The renal medulla is made up by tubular portions of the Henle loop, including thick, thin, and collecting tubules.

Bone histology was also performed to show that scaffolds promoted bone healing in damaged areas (Fig. 3). New trabecular bone was observed to have formed at defect site 21 days later (Figs. 3(b) and

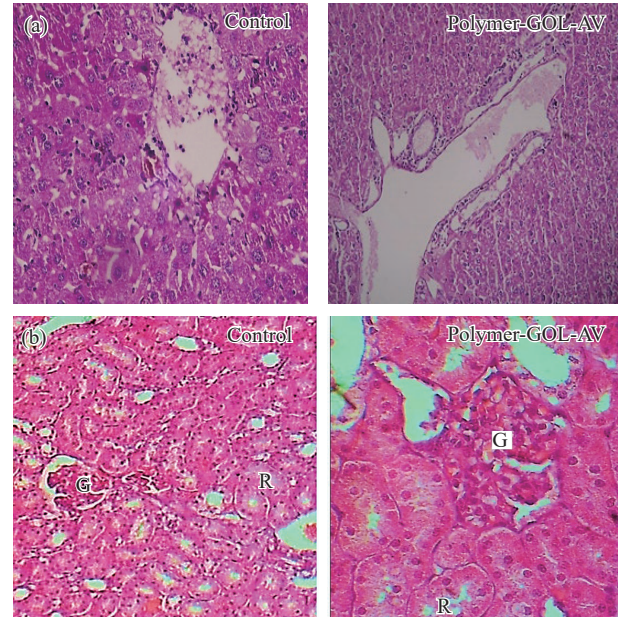


Fig. 2 Assessment of scaffold toxicity to liver and kidney tissue. Section of renal cortex shows a normal appearance of glomerulus (G) & renal tubules (R). Hematoxylin and eosin (H&E) stain.

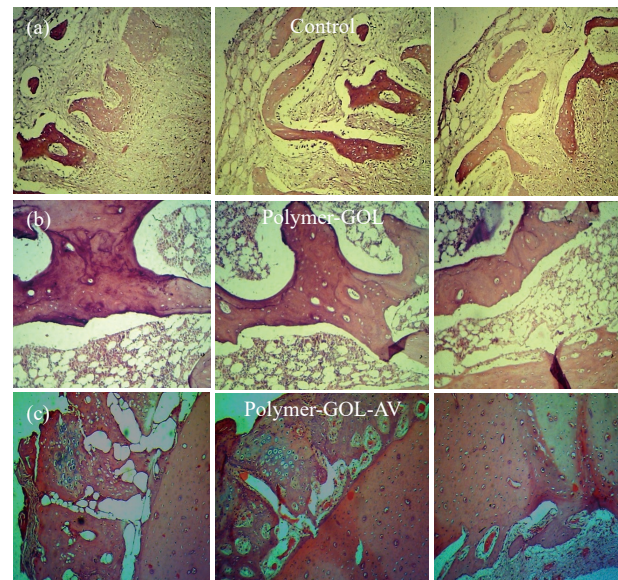


Fig. 3 Effect of scaffolds on bone healing using as imaged using histological sections.

3(c)). Moreover, relative to the control group (Fig. 3(a)), scaffold implantation at the defect site resulted in a significant increase in the production of new trabecular bone. Histopathological examination of the treatment groups at the end of the 6th week postoperation revealed an increase in trabecular bone formation. This new tissue appeared mature, wide, and well mineralized with small cavities within the trabecula. In contrast, in the control groups, we observed a thin and less mineralized trabecula bone formation that contained a much larger cavity. At the

end of the 12th week postoperation, we observed a mature trabecula bone formation in the treatment groups. This featured a well mineralized, widening, and lamellar bone formation, circling the bony device and partially incorporating it into the bone. We also observed that the empty osteocyte lacunae of the bony device were filled with osteocytes, and blood vessels had invaded the haversian canal. In contrast, in the control group, the trabecula bone was thin and less mineralized and showed many cavities. Here, the wound site had not yet converted to lamellar bone, and some of the empty lacunae within the bony device were still not yet filled with osteocytes. Finally, we also observed an increase in the diameter of the haversian canal. Next, we performed physical and mechanical analyses. These results revealed that the bone of the treatment group was denser and harder than that of the control group. Moreover, when exposed to pressure and heat to analyze fracture tolerance, our results showed that the bone of the treatment group was more resistant to pressure and could tolerate a higher fracture load than the control group.

Next, the Runx2-mediated modulation of gene expression of the bone biomarkers ALP and OCN was investigated to determine the mechanisms responsible for scaffold-induced improvement in bone repair (Fig. 4). ALP was immunodetected at the injury site of right femurs 21 days after the induction of the bone defects (Fig. 4). Moreover, the implantation of scaffolds into the bone defect region of the left femur showed a noticeable increase in ALP levels. Similarly, OCN was immunodetected at the bone defect site of the right femur, resulting in a significant increase in OCN levels (Fig. 4). In addition, scaffold administration elevated the ALP

and OCN levels at the bone defect locations. As internal controls, we also examined actin concentrations, and performed quantification and statistical analysis of the resulting protein bands. Our estimates showed that the scaffolding generated large increases in ALP and OCN levels of approximately 160% and 90%, respectively, after implantation.

Scaffolds can promote bone healing by inducing ALP and OCN expression. ALP levels at the injury site rose after scaffolds were installed. This is significant because ALP, a common bone marker, is involved in the regulation of osteoblast activity, and the proliferation and maturation of osteoblasts are both accelerated when ALP is increased. Our previous findings confirmed that polymer-GOL-VA can induce osteoblast development and mineralization. In addition, after treatment with scaffolds, the level of OCN at the bone defect site increased. OCN is an early osteoblast marker that regulates bone ECM mineralization and development. Moreover, Runx2 has been shown to affect the transcription of both the *OCN* and *ALP* genes. Runx2 also enhances the differentiation of multipotential mesenchymal ROB-C26 cells into mature osteoblasts via modulating *OCN* and *ALP* gene expression, as reported previously [20]. We therefore speculate that scaffolds may upregulate Runx2 levels at the site of bone injury, thereby causing OCN and ALP expression. The final phases of the osteogenesis process involve extracellular matrix (ECM) mineralization and osteoblast maturation. The effect of scaffolds on improving osteoblast mineralization has been demonstrated by a prior study [18]. As a result, our findings suggest that scaffold implantation enhances osteogenesis and bone repair via inducing Runx2-mediated ALP and OCN expression. Our data

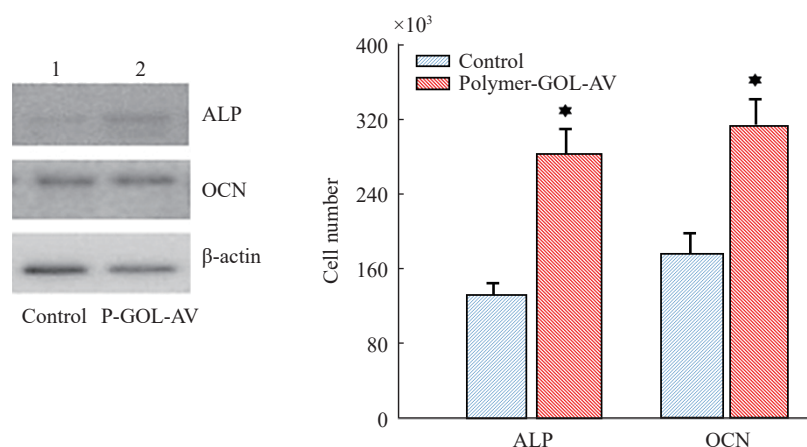


Fig. 4 Effects of polymer-GOL-AV scaffolds on ALP and OCN in bone fracture.

show that the scaffolds obtained here had high porosities (e.g., 70%–90%) and large macro pore sizes of 100–500 μm (Fig. 5). In addition, tissue sections revealed inflammatory cell attack and surface decomposition after transplantation, but this effect had dissipated by 3–20 days after transplantation.

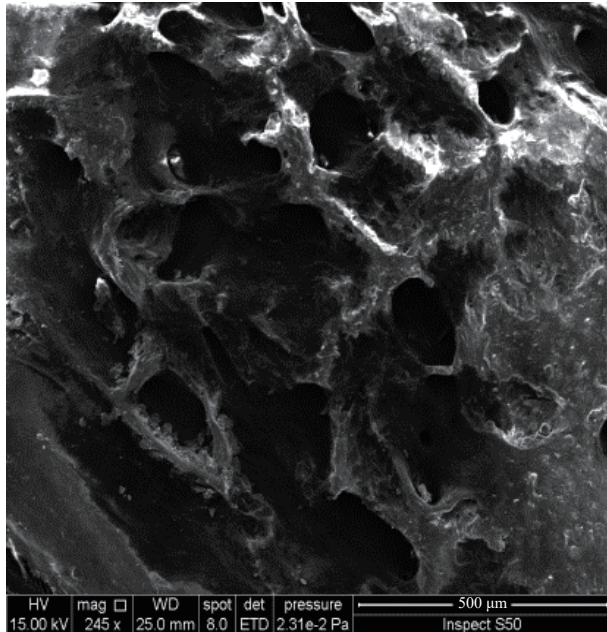


Fig. 5 Field emission scanning electron microscopy (FESEM) image of scaffold.

Conclusion

This study established an animal model to investigate the effects of composite scaffolds on bone repair. Our results revealed that scaffolds show positive effects on bone remodeling, fixation, and the creation of new trabecular bone. Histological analyses indicated increased levels of OCN and ALP at the site of bone injury after scaffold implantation, and their promoting bone healing by increasing trabecular bone formation, thickness, and cellular connections. The molecular processes responsible for scaffold-induced bone healing may be related to Runx2-mediated modulation of *ALP* and *OCN* gene expression. Therefore, our research suggests that scaffolds might be clinically beneficial for treating bone abnormalities and fractures related to osteoporosis.

CRedit author statement

Marwa Abdul Muhsien Hassan: Formal analysis,

Funding acquisition, Writing (review and editing). **Asmaa Hadi Mohammed:** Supervision, Writing (original draft). **Ekhlas Majeed Hameed:** Methodology, Software.

Conflict of Interest

The authors declare that no competing interest exists.

References

- [1] E.García-Gareta, M.J. Coathup, G.W. Blunn. Osteoinduction of bone grafting materials for bone repair and regeneration. *Bone*, 2015, 81: 112–121. <https://doi.org/10.1016/j.bone.2015.07.007>
- [2] V.L. Zizzari, S.Z. Zara, G. Tetè, et al. Biologic and clinical aspects of integration of different bone substitutes in oral surgery: a literature review. *Oral Surgery Oral Medicine, Oral Pathology and Oral Radiology*, 2016, 122(4): 392–402. <https://doi.org/10.1016/j.oooo.2016.04.010>
- [3] A.C. Baptistel, J.M.C.P. Coutinho, E.M.F. Lins Neto, et al. Plantas medicinais utilizadas na Comunidade Santo Antônio, Currais, Sul do Piauí: um enfoque etnobotânico. *Revista Brasileira de Plantas Medicinais*, 2014, 16: 406–425. (in Portuguese) https://doi.org/10.1590/1983-084X/12_137
- [4] C.E. Rios, A.G. Abreu, J.A. Braga Filho, et al. *Chenopodium ambrosioides* L. improves phagocytic activity and decreases bacterial growth and the systemic inflammatory response in sepsis induced by cecal ligation and puncture. *Frontiers in Microbiology*, 2017, 8: 148. <https://doi.org/10.3389/fmicb.2017.00148>
- [5] M.A. Ghareeb, A.M. Saad, A.M. Abdou, et al. A new Kaempferol glycoside with antioxidant activity from *Chenopodium ambrosioides* growing in Egypt. *Oriental Journal of Chemistry*, 2016, 32: 3053–3061. <https://doi.org/10.13005/ojc/320626>
- [6] K. Drzewiecka, J. Krasowski, M. Krasowski, et al. Mechanical properties of composite material modified with amorphous calcium phosphate. *Journal of Achievements in Materials and Manufacturing Engineering*, 2016, 74(1): 22–28. <https://doi.org/10.5604/17348412.1225754>
- [7] B. Bisht, A. Hope, A. Mukherjee, et al. Advances in the fabrication of scaffold and 3D printing of biomimetic bone graft. *Annals of Biomedical Engineering*, 2021, 49: 1128–1150. <https://doi.org/10.1007/s10439-021-02752-9>
- [8] J.A. McGovern, M. Griffin, D.W. Huttmacher. Animal models for bone tissue engineering and modelling disease. *Disease Models & Mechanisms*, 2018, 11(4): dmm033084. <https://doi.org/10.1242/dmm.033084>
- [9] B. Shen, K. Vardy, P. Hughes, et al. Integrin alpha11 is an Osteolectin receptor and is required for the maintenance of adult skeletal bone mass. *eLife*, 2018 e42274. <https://doi.org/10.7554/eLife.42274>
- [10] D. Zhao, R. Liu, G. Li, et al. Connexin 43 channels in osteocytes regulate bone responses to mechanical unloading. *Frontiers in Physiology*, 2020, 11: 299. <https://doi.org/10.3389/fphys.2020.00299>
- [11] T. Ghassemi, A. Shahroodi, M.H. Ebrahimzadeh, et al. Current concepts in scaffolding for bone tissue engineering. *The Archives of Bone and Joint Surgery*, 2018, 6(2): 90–99.

- [12] D. Zhang, X. Wu, J. Chen, et al. The development of collagen based composite scaffolds for bone regeneration. *Bioactive Materials*, 2018, 3(1): 129–138. <https://doi.org/10.1016/j.bioactmat.2017.08.004>
- [13] S. Fiorilli, C. Pontremoli, G. Montalbano, et al. Hybrid formulations based on mesoporous bioactive glasses/polymeric phases for the design of bone scaffolds and delivery platforms. In: *Bioactive Glasses—Properties, Composition and Recent Applications*. D. Arcos, M. Vallet-Regi, eds. NOVA: Nagoya, 2020: 412.
- [14] S. Fiorilli, G. Molino, C. Pontremoli, et al. The incorporation of strontium to improve bone-regeneration ability of mesoporous bioactive glasses. *Materials*, 2018, 11(5): 678. <https://doi.org/10.3390/ma11050678>
- [15] G. Montalbano, G. Borciani, C. Vitale-Brovarone, et al. Collagen hybrid formulations for the 3D printing of nanostructured bone scaffolds: An optimized genipin-crosslinking strategy. *Nanomaterials*, 2020, 10: 1681. <https://doi.org/10.3390/nano10091681>
- [16] J.R. Perez, D. Kouroupis, D.J. Li, et al. Tissue engineering and cell-based therapies for fractures and bone defects. *Frontiers in Bioengineering and Biotechnology*, 2018, 6: 105. <https://doi.org/10.3389/fbioe.2018.00105>
- [17] M. Soltani, P. Alizadeh. *Aloe vera* incorporated starch-64S bioactive glass-quail egg shell scaffold for promotion of bone regeneration. *International Journal of Biological Macromolecules*, 2022, 217: 203–218. <https://doi.org/10.1016/j.ijbiomac.2022.07.054>
- [18] S. Boonyagul, W. Banlunara, P. Sangvanich, et al. Effect of acemannan, an extracted polysaccharide from *Aloe vera*, on BMSCs proliferation, differentiation, extracellular matrix synthesis, mineralization, and bone formation in a tooth extraction model. *Odontology*, 2014, 102(2): 310–317. <https://doi.org/10.1007/s10266-012-0101-2>
- [19] M.A.M. Hassan, A.H. Mohammed, Z. K. Hamzh. Potential role of laser therapy on scaffold implantation for osteogenesis and regeneration with microbial protection. *BioNanoScience*, 2022, 12: 1059–1085. <https://doi.org/10.1007/s12668-022-01033-6>
- [20] R. Senthil, S.B. Kavukcu. Efficacy of glycoprotein-based nanocurcumin/silk fibroin electrospun scaffolds: Perspective for bone apatite formation. *Materials Chemistry and Physics*, 2022, 289: 126444. <https://doi.org/10.1016/j.matchemphys.2022.126444>
- [21] R. Senthil, Ç. Sinem, S.B. Kavukcu, et al. Fabrication of cylindrical bone graft substitute supported by reduced graphene-oxide and nanocurcumin to promotes the bone tissue development. *Materials Letters*, 2022, 322: 132475. <https://doi.org/10.1016/j.matlet.2022.132475>
- [22] S. Rethinam, S. Vijayan, B. Basaran, et al. Enhanced tissue regeneration using an nano-bioactive scaffold-A novel perspective. *Materials Chemistry and Physics*, 2020, 240: 122303. <https://doi.org/10.1016/j.matchemphys.2019.122303>

© The author(s) 2023. This is an open-access article distributed under the terms of the Creative Commons Attribution 4.0 International License (CC BY) (<http://creativecommons.org/licenses/by/4.0/>), which permits unrestricted use, distribution, and reproduction in any medium, provided the original author and source are credited.